International Journal of Research Studies in Electrical and Electronics Engineering(IJRSEEE)
Volume 4, Issue 3, 2018, PP 18-25
ISSN 2454-9436 (Online)
DOI: http://dx.doi.org/10.20431/2454-9436.0403003
www.arcjournals.org

Review of Surface Plasmon Polaritons in Nanostructured Metamaterials

Tatjana Gric*

Department of Electronic Systems, Vilnius Gediminas Technical University, Vilnius, Lithuania
Semiconductor Physics Institute, Center for Physical Sciences and Technology, Vilnius, Lithuania

***Corresponding Author:** ***Tatjan Gric**, Department of Electronic Systems, Vilnius Gediminas Technical University, Vilnius, Semiconductor Physics Institute, Center for Physical Sciences and Technology, Lithuania*

Abstract: *Herein, we discover the new kinds of surface wave on nanostructured metamaterial (MM), crossing the light line with a substantial portion at lower frequencies lying above the free space light line. Interestingly, the propagation of such surface waves is found to be sensitive to the parameters of the materials employed in nanostructures. Furthermore, the Ferrel-Berreman modes are observed under the certain conditions, opening a gateway towards device fabrications.*

1. INTRODUCTION

The presence of electromagnetic waves on two-dimensional interfaces has been extensively studied over the last several decades [1, 2]. Surface plasmonic polariton (SPP) [3], which normally exists at the interface between a noble metal and a dielectric, is treated as the most widely investigated surface wave. SPPs have promoted new applications in many fields such as microelectronics [4], photovoltaics [5], near-field sensing [6], laser technology [7], photonics [8], meta-materials design [9], high order harmonics generation [10], or charged particles acceleration [11]. Recently, it has been shown that by nanostructuring the metal surface, it is possible to modify the dispersion of SPPs or excite the SPPs in a prescribed manner. Hyperbolic MMs [12], being special kind of anisotropic MM with dielectric tensor elements having the mixed signs, have attracted growing attention due to their ability to support very large wave vectors. Their exotic features give rise to many intriguing applications, such as sub-wavelength imaging and hyper-lens that are infeasible with natural materials.

Herein, we discover the new kinds of surface wave on nanostructured MM, crossing the light line with a substantial portion at lower frequencies lying above the free space light line. Interestingly, the propagation of such surface waves is found to be sensitive to the parameters of the materials employed in nanostructures. Furthermore, the Ferrel-Berreman modes are observed under the certain conditions, opening a gateway towards device fabrications.

2. TUNABLE HYPERBOLIC MM MADE OF GRAPHENE-DIELECTRIC MULTILAYERS

Let us consider a hyperbolic MM heterostructure consisting of stacked graphene sheets separated by dielectric layers, as shown schematically in Fig. 1.

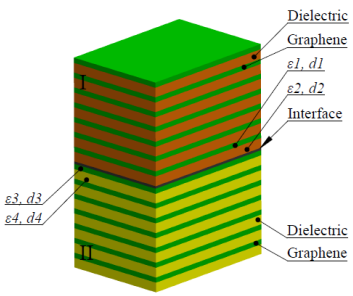

Fig1. *Schematic view of an interface separating two different infinite layered nanoctructured MMs formed by alternating graphene and dielectric layers. Herein, indexes "1, 2" correspond to the graphene and dielectric layers correspondingly.*

To describe the optical response of such a system, we apply the effective-medium approach [13] which is justified if the wavelength of the radiation considered is much larger than the thickness of any layer.

In this section we present dispersion curves computed after performing the homogenization of two HMs. Thus, in Fig. 2 the dispersion curves for the case $\varepsilon_1 = \varepsilon_3$, $\varepsilon_2 = \varepsilon_4$ and $d_1 \neq d_2 \neq d_3 \neq d_4$ are reported. The dispersion curves of spoof SPPs at the boundary of two MMs with d_1=0.35nm, d_2=10nm, d_3=0.25nm, d_4=10.1nm are shown in Fig. 2. Moreover, it should be mentioned, that Figure 2 gives the dispersion of surface waves with the effective parameters presented in [13].

The frequency ranges of surface wave can be tuned by changing the Fermi energy, which is consistent with the dependence of the $\varepsilon_\perp$ on the Fermi energy [13]. It should be mentioned that decreases in the Fermi energy μ will move the dispersion curves to lower frequencies; in contrast, increases in the Fermi energy μ move them to higher frequencies. As seen from Fig. 2, the smallest asymptotic frequency is achieved by employing the smallest Fermi energy. The former tunability property suggests that the surface wave can be engineered by the Fermi energy of the graphene sheets. It should be mentioned, that SPP excitations match the part of the dispersion curves lying to the right of the light line due to their bound nature. Consequently, special phase-matching techniques such as a grating or prism coupling [14], near-field excitation [15], and end-fire coupling [16] are required for their excitation via three-dimensional beams [3]. Between the regime of the bound and radiative modes, a frequency gap region with purely imaginary β prohibiting propagation exists.

As the graphene is not modeled as lossless, β is complex, leading to a finite propagation length, drawn in Fig. 2(b).

Turning now to the second case under in our study, i. e. $\varepsilon_1 = \varepsilon_3$, $\varepsilon_2 \neq \varepsilon_4$ and $d_1 \neq d_2 \neq d_3 \neq d_4$, in Fig. 3 four modes are represented at the boundary of two different MMs with ε_4=2.25. As seen from Fig. 3, the smallest asymptotic frequency corresponds to the case $\mu = 0.5$ eV. Compared with the dispersion relation of depicted in Fig. 2, it can be seen that the bound SPPs approach now a maximum, finite wave vector at the surface plasmon frequency of the system. Also, the quasi-bound [17], leaky part of the dispersion relation is allowed due to the fact, that Re (β)≠0. Thus β does not tend to infinity as the surface plasmon frequency is approached, but folds back and eventually crosses the light line.

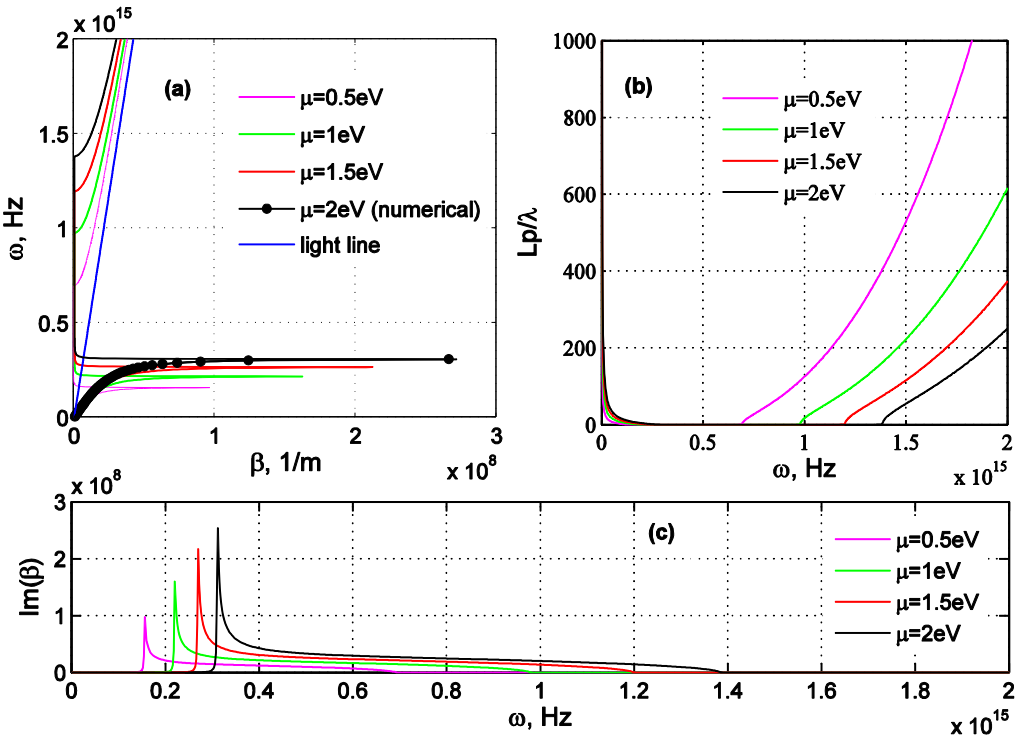

Fig2. *The dispersion of surface waves (a); propagation lengths (b) and absorption (c) at different Fermi energy, where N=1, d_d=10 nm, $\varepsilon_1 = \varepsilon_3$, $\varepsilon_2 = \varepsilon_4$ and $d_1 \neq d_2 \neq d_3 \neq d_4$ and the blue line in (a) is the free-space light line.*

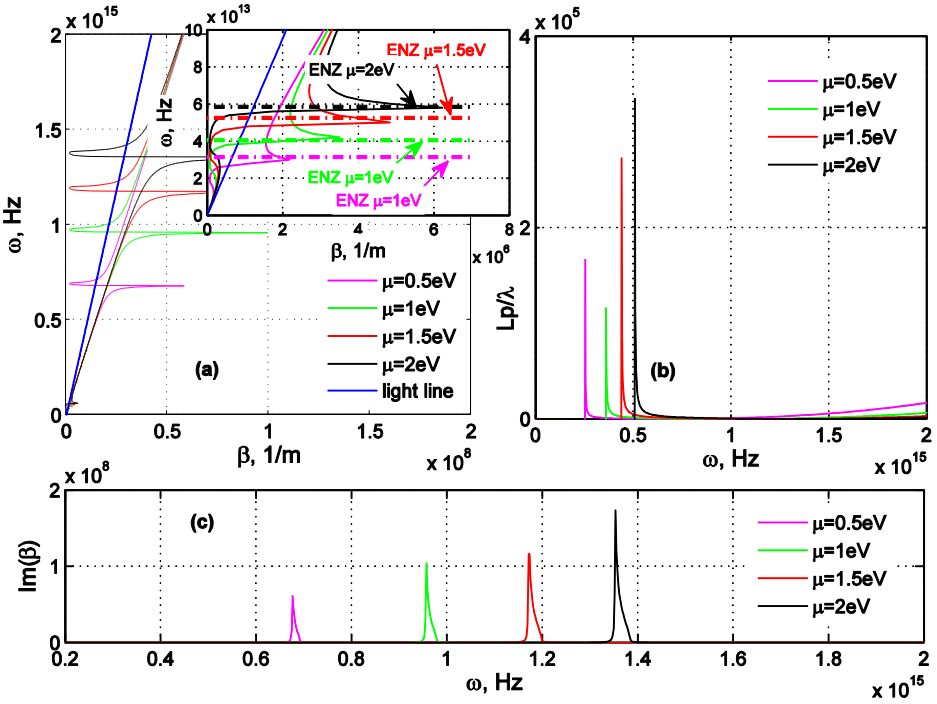

Fig3. *The dispersion of surface waves (a); propagation lengths (b) and absorption (c) at different Fermi energy, where N=1, d_d=10 nm, $\varepsilon_1 = \varepsilon_3$, $\varepsilon_2 \neq \varepsilon_4$ and $d_1 \neq d_2 \neq d_3 \neq d_4$ and the blue line in (a) is the free-space light line.*

As in previous cases, the case denoted as $\varepsilon_1 = \varepsilon_3$, $\varepsilon_2 \neq \varepsilon_4$ and $d_1 = d_3$, $d_2 = d_4$ will be illustrated by means of the dispersion diagrams of the TM modes. In Fig. 4, four different modes are presented. It is of particular interest to examine the effect of controlling the fill factors of the dielectric and graphene sheet as shown in Fig. 4. First, we discuss the influence of the thickness of the dielectric d_d on the dispersion curve (see Fig 4(a)). We find that the upper limit moves to the higher frequencies as d_d is increased. This is consistent with the effect of d_d on the frequency range of $\varepsilon_\perp$. Moreover, the frequency range for surface waves can also be controlled by increasing the number of graphene layers, as shown in Fig. 4 (c). The dependence of the frequency range in which surface waves exist on the thickness of dielectric and layer number of graphene sheets provides an unprecedented degree of freedom to control the surface wave at the near-infrared frequencies.

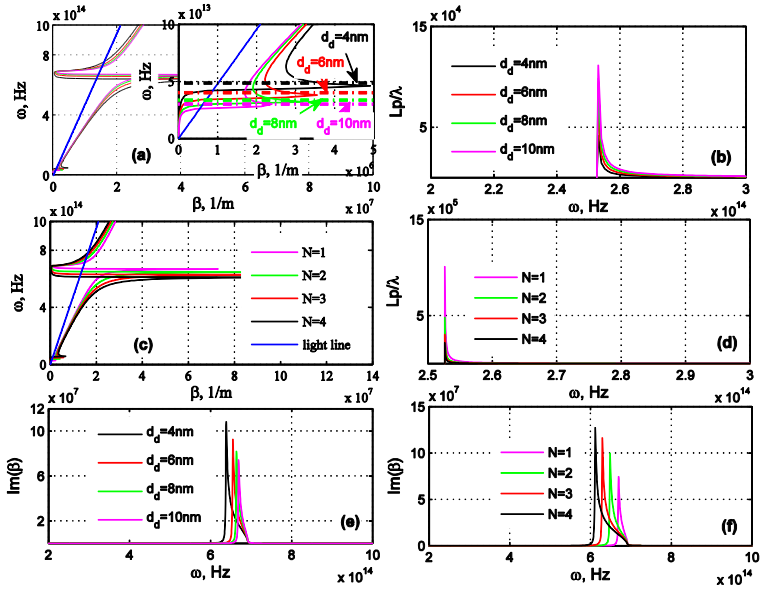

Fig4. *The dependences of dispersion of surface waves, propagation lengths and absorption on (a), (b), (e) the thickness of dielectric d_d and (c), (d), (f) number of graphene sheets. Herein N=1, μ=0.5eV in (a), (b), (e) and d_d=10nm, μ=0.5eV in (c), (d), (f).*

It should be mentioned, that negative values of the electrical length and absorption in Figs. 2(b), 2(c), 3(b), 3(c), 4(b), 4(d)-4(f) which result from non-physical solutions of the dispersion equation and have been omitted in line with [18]. Moreover, the sketched graphs imply the presence of the surface waves propagating for a long distance. This is caused by the fact that the real part of β is very low within this spectral region. It should be taken into account, that the same phenomena takes place in case of the interface separating uniaxial MM and isotropic medium [19].

The imaginary parts of the wave vector (i. e. absorption) are plotted in Figs. 2(c), 3(c), 8(e), 8(f). Taking advantage of the absorption resonances, one can show that the simple multilayer structures without possessing any periodic corrugation have the prospective to act as directive and monochromatic thermal sources [20].

By presenting a modal analysis, we now show that the physical origin of the bulk absorption in MMs is due to the excitation of leaky bulk polaritons called Ferrel-Berreman modes [21-23]. As a matter of fact, volume charge oscillations at the ENZ of the metal (bulk or volume plasmons) are formed by the bulk metal. The important property to note now is that these excitations are in the form of a completely longitudinal wave and hence cannot be excited with free space light (which a transverse wave). The top and bottom interface couple in case of films of metal with thicknesses less than the metal skin depth, permitting for collective charge oscillations across the film. In such a case, the bulk plasmon is no longer purely longitudinal and can interact with free space light at frequencies near the metal ENZ [24]. Ferrell addressed this approach for metallic foils in [25], Berreman - for polar dielectric films in [26]. Radiative excitations which we call FB modes are supported by the multilayer MMs with the employed graphene layers. It is worthwhile mentioning, that these FB modes are different from surface plasmon polaritons supported by metal foils, due to the reason that in case of surface plasmon modes, energy propagates along the surfaces of the metal, whereas in FB modes volume charge oscillations are setup across the foil and energy propagates within the bulk of the metal. The bulk polaritons under consideration have transverse wave vectors similar to free space light and exist to the left of the light line. Thus, in Figs. 2(a), 3(a), 3(c) it is interesting to observe the FB modes which exist at energies near the ENZ of the hyperbolic MM to the left of the light line.

3. TUNABLE HYPERBOLIC MM MADE OF TRANSPARENT CONDUCTING OXIDE-DIELECTRIC MULTILAYERS

The structure of the MM studied here is shown in Fig. 5, where d_{TCO} and d_d represent the thicknesses of the transparent conducting oxide (TCO) and dielectric layers, respectively. All the involved media are assumed as nonmagnetic (so the magnetic permeability of every medium is the same as that of vacuum). In our numerical calculation, we use a semi-infinite TCO/PbS MM as an example to explore the dispersive features of HSPPs, where ε_d=18.8 for PbS layers, and ε_{TCO} is calculated using the parameters presented in [27].

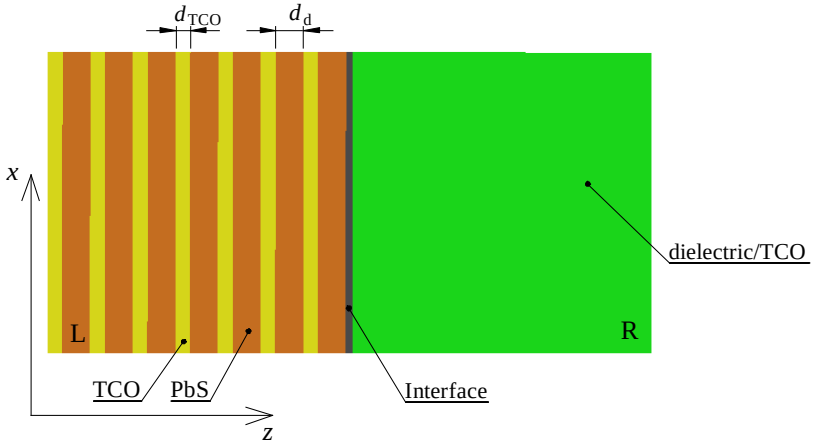

Fig5. *One-dimensional MM composed of alternating TCO and dielectric layers. The MM/dielctric ($\varepsilon_R = 1$ or $\varepsilon_R = 2.25$) and MM/TCO interfaces are considered.*

In the case of a spatially infinite anisotropic material, invariant in two directions, the electromagnetic wave dispersions can be plotted for both, the MM/dielectric and the MM/TCO case. Assuming a homogenization of the MM corresponding to the MM/dielectric and MM/TCO interfaces let us, as an

example when performing the numerical calculations, focus on a semi-infinite AZO/PbS MM. We shall first review the optical properties by depicting the curves of the principal values ($\varepsilon_{\perp}$ and $\varepsilon_{\parallel}$) and the dielectric constant (ε_R) and subsequently distinguish different frequency regions according to the properties of and relation among $\varepsilon_{\perp}$, $\varepsilon_{\parallel}$ and ε_R [28].

(1) $\varepsilon_{\perp} > \varepsilon_R > \varepsilon_{\parallel}$ and $\varepsilon_{\parallel} < 0$ (cyan);

(2) $\varepsilon_{\perp} > \varepsilon_R > \varepsilon_{\parallel}$ (green);

(3) $\varepsilon_{\parallel} > \varepsilon_R > \varepsilon_{\perp}$ and $\varepsilon_{\perp} < 0$ (gray),

(4) $\varepsilon_R > \varepsilon_{\parallel} > \varepsilon_{\perp}$ and $\varepsilon_{\perp} < 0$ (magenta) and

(5) $\varepsilon_{\perp} < \varepsilon_{\parallel} < 0$ (orange).

Clearly, a tuning of the effective parameters will have an effect on the dispersion curves of the HSPPs as presented in [28]. The parameter which principally defines such a tunability of the effective optical parameters of our MM is the TCO filling ratio, f_{TCO}. Fig. 6 and Fig. 7 show characteristic dispersion curves for various TCO filling ratios. The curve colors correspond to different frequency regions. For f_{TCO}=0.3, there are three HSPPs belonging to three different kinds, associated with the case of a MM/dielectric interface and two kinds of HSPPs in case of MM/TCO interfaces, respectively. The upper waves exist in the gray region for the MM/TCO case. Three exceptional cases are related to f_{TCO}=0.5, 0.7, 0.9. In case of f_{TCO}=0.5, two kinds of HSPPs exist in two color regions, i.e. cyan and gray for MM/dielectric and MM/TCO interfaces. The upper short curves in the case of f_{TCO}=0.7 lie in the gray region, as illustrated in Figs. 6, 7. The other HSPPs lie in the orange region. The additional HSSPs lying in the magenta region correspond to the case of a MM/dielectric interface. The extension of the magenta range for the case $\varepsilon_R = 2.25$ is displayed by a dark-magenta color. In the case of f_{TCO}=0.9, two kinds of HSPPs are found lying in the orange and cyan regions for MM/TCO case and three kinds of HSPPS lying in the cyan, orange and gray regions for the MM/dielectric case. Fig. 6 also demonstrates that there always is one HSPP in the cyan region for various TCO filling ratios in MM/dielectric case. It is worthwhile mentioning, that the case $\varepsilon_R = \varepsilon_{ITO}$ also allows for the rich phenomenon as the HSPP always exists in the cyan region for various filling ratios (Fig. 7).

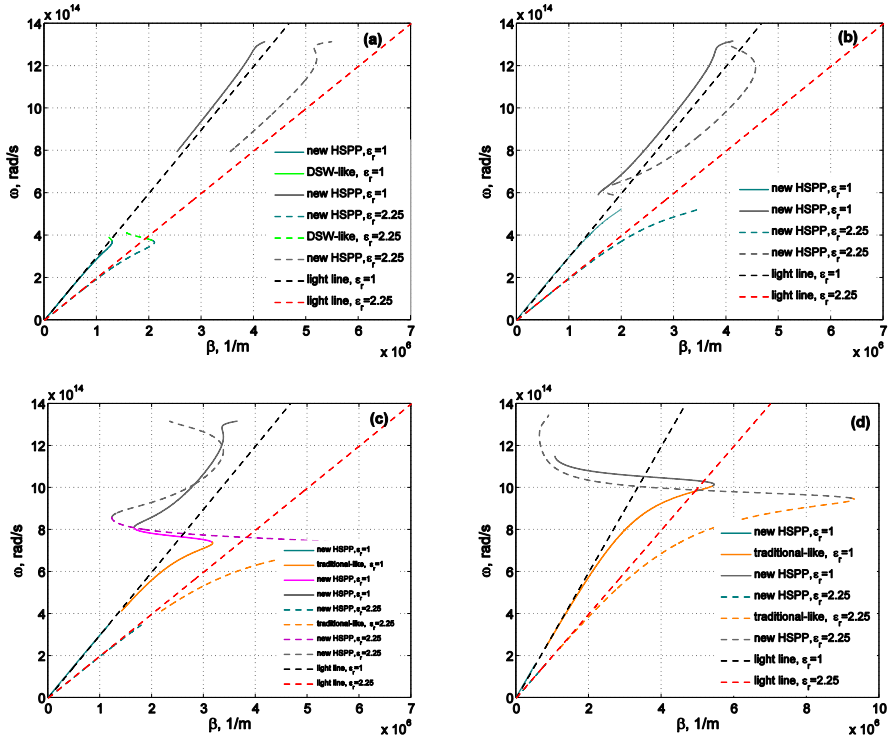

Fig6. *Dispersion curves of HSPPs for various TCO filling ratios, i. e.* $f_{TCO} = 0.3$ *in (a),* $f_{TCO} = 0.5$ *in (b),* $f_{TCO} = 0.7$ *in (c),* $f_{TCO} = 0.9$ *in (d), corresponding to the MM/dielectric interface.*

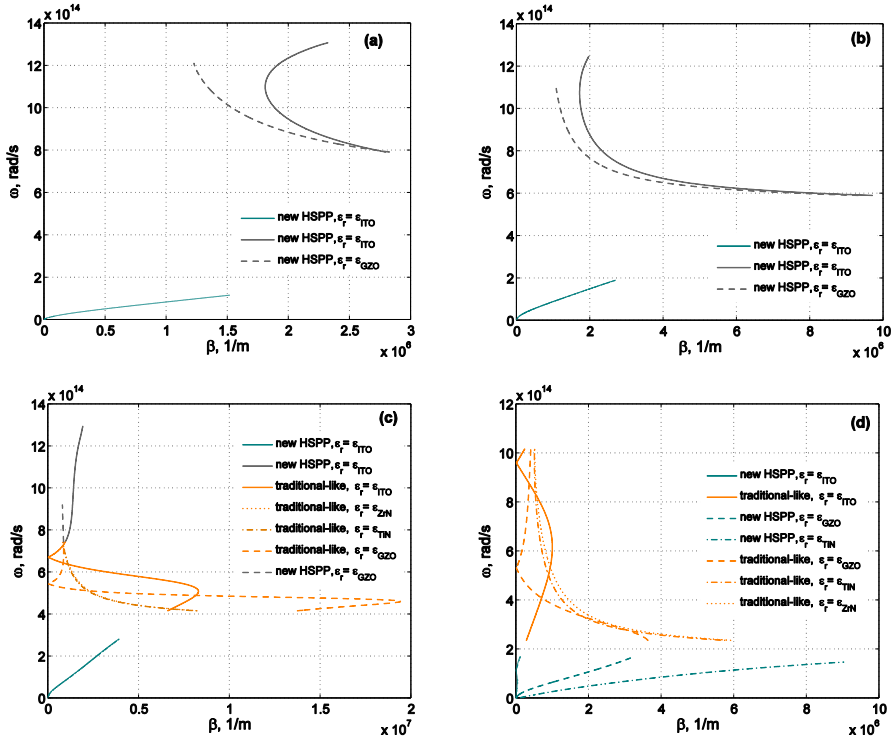

Fig7. *Dispersion curves of HSPPs for various TCO filling ratios, i. e.* $f_{TCO} = 0.3$ *in (a),* $f_{TCO} = 0.5$ *in (b),* $f_{TCO} = 0.7$ *in (c),* $f_{TCO} = 0.9$ *in (d), corresponding to the MM/TCO interface.*

Based on the necessary condition for the existence of the DSW [29], the HSPP in the green region (Fig. 6) is similar to the DSW so it is appropriate to be associated with a Dyakonov-like SPP [30], or the Dyakonov defined in [29]. Moreover, we can extend the frequency range of the DSW existence by replacing the material at the right-hand side of the interface with $\varepsilon_R = 2.25$ (Fig. 6). The former extension is demonstrated by the dark-green color [28]. It is worthwhile mentioning, that extension of the gray region [28] is possible due to the employment of ITO instead of GZO at the right-hand side of the interface (the extension of the gray range is depicted by the light-gray color). Due to the negative principal values of the effective permittivity in the orange region, the HSPP in this region is similar to the traditional SPP, so we should associated it with an SPP of traditional type. The others are new types of HSPPs. Thus, all the HSPPs are divided into five kinds, situated in the five color regions in Figs. 6, 7, respectively. In case of AZO/PbS MM and air/dielectric interface 5 types of the HSPPs exist, and only 3 are seen in case of AZO/PbS MM and TCO interface.

As expected, a traditional-like SPP has a typical dispersion in case of the MM/dielectric interface, lying to the right of the light line. At the same time, the degradation of the dispersion in the orange region takes place in case of the MM/TCO interface. The dispersion properties can be tuned with the TCO filling ratio of the MM realization. While for a low TCO filling ratio in case of the MM/TCO interface, two types of the modes are always present, whereas for higher TCO filling ratios, modes in the gray region vanish (Fig. 7(d)).

It is worthwhile noting, that the complex mode structure (Figs. 6, 7) corresponding to either MM/dielectric or MM/TCO interface emerges as a consequence of the confinement of plasmon-polaritons in the direction perpendicular to the wave propagation. These electromagnetic surface waves arise via the coupling of the electromagnetic fields to oscillations of the conductor's electron plasma.

4. CONCLUSION

In conclusion, we have outlined a method to investigate the dispersion diagrams of hyperbolic MMs. This work aims at providing a comprehensive and updated picture suggesting a dynamic control of the hyperbolic properties, which is extremely desirable in view of device applications. In summary, a graphene-based layered structure treated as the hyperbolic MM is presented. We provided the dispersion relations for various cases, and discussed the controllable properties of the effective

permittivity of the graphene-based HMs. There are three important conclusions that can be drawn from results presented here (i) Compared with the dispersion relation in case of $\varepsilon_1 = \varepsilon_3$, $\varepsilon_2 = \varepsilon_4$ and $d_1 \neq d_2 \neq d_3 \neq d_4$, the quasibound, leaky part of the dispersion relation is narrowed for the case $\varepsilon_1 = \varepsilon_3$, $\varepsilon_2 \neq \varepsilon_4$ and $d_1 \neq d_2 \neq d_3 \neq d_4$ (ii) the perpendicular component of effective permittivity can be tuned by changing the Fermi energy applied on the graphene sheets, the thickness of dielectric, and the number of layers of graphene sheets in HMs (iii) the frequency range of surface wave existence can be engineered by varying the Fermi energy of graphene and the fill factor of dielectric or graphene sheets in the unit cell of HMs. We have investigated hybrid surface plasmon polaritons (HSPPs) in a one-dimensional transparent conducting oxide (TCO)-dielectric MM. Similar to graphene-dielectric MM [13], TCO-dielectric MM support traditional-like SPPs having different patterns corresponding to two different interfaces. The dispersion equations of HSPPs are obtained based on the theoretical approach [30]. Five kinds of HSPP, among which three kinds are new types of HSPPs and one is the Dyakonov-like SPP and another is the traditional-like SPP are predicted. The existence of these HSPPs is dramatically influenced by the properties of and the relation among the principal values of the effective permittivity and the dielectric constant of the covering medium. It is worthwhile mentioning that the (new) types of the HSPPs discussed here arise because the principal values of the effective pemittivity are functions of frequency and can be negative or positive. Moreover, we predict surface modes with a dispersion that coincides with the dispersion of a surface plasmon at the boundary of two isotropic media corresponding to the MM interface if the material at the right-hand side is the same as employed in the MM.

REFERENCES

[1] C. J. Zapata-Rodrı´guez, J. J. Miret, S. Vukovic´, M. R. Belic´, Opt. Express **21**, 19113–19127 (2013).

[2] Z. Jacob, E. E. Narimanov, Appl. Phys. Lett. **93**, 221109 (2008).

[3] S. A. Maier, *Plasmonics, Fundamentals and Applications*, Springer, 2007.

[4] K. F. MacDonald, Z. L. Samson, M. I. Stockman, N. I. Zheludev, Nat. Photonics **3** (1), 55–58 (2009).

[5] H. A. Atwater, A. Polman, Nat. Mater. **9**, 205–213 (2010).

[6] A. Kabashin, P. Evans, S. Pastkovsky, W. Hendren, G. Wurtz, R. Atkinson, R. Pollard, V. Podolskiy, A. Zayats, Nat. Mater. **8**, 867–871 (2009).

[7] Y. Park, S. Kim, J. Choi, D.-H. Lee, Y.-J. Kim, M. F. Kling, M. I. Stockman, S.-W. Kim, Nat. Photonics **5** (11), 677–681 (2011).

[8] W. Barnes, A. Dereux, T. Ebbesen, Nature **424**, 824–830 (2003).

[9] V. M. Shalaev, Nat. Photonics **1**, 41–48 (2007).

[10] S. Kim, J. Jin, Y.-J. Kim, I.-Y. Park, Y. Kim, S.-W. Kim, Nature **453** (7196), 757–760 (2008).

[11] P. Genevet, J.-P. Tetienne, E. Gatzogiannis, R. Blanchard, M. A. Kats,M. O. Scully, F. Capasso, Nano Lett. **10** (12), 4880–4883 (2010).

[12] V. P. Drachev, V. A. Podolskiy, A. V. Kildishev, Opt. Express, **21**(1), 15048-15064 (2013).

[13] T. Gric, O. Hess, Opt. Express **25**(10), 11466-11476 (2017).

[14] E. Kretschmann, H. Raether, Z Naturforsch **23A**, 2135-2136 (1968).

[15] B. Hecht, H. Bielefeld, L. Novotny, Y. Inouye, D. W. Pohl, Phys. Rev. Lett. **77**, 1889-1892 (1996).

[16] J. Tian, S. Yu, W. Yan, M. Qiu, Appl. Phys. Lett. **95**, 013504 (2009).

[17] J. A. Dionne, L. A. Sweatlock, H. A. Atwater, A. Polman, Phys. Rev. B **72**(7), 075405 (2005).

[18] R. T. Ling, J. D. Scholler, P. Ya. Ufimtsev, Pr. Electromaghn. Res. **19**, 49-91 (1998).

[19] J.A. Sorni, M. Naserpour, C.J. Zapata-Rodríguez, J. J. Miret, Opt. Commun. **355**, 251-255 (2015).

[20] S. Campione, F. Marquier, J.-P. Hugonin, A. R. Ellis, J. F. Klem, M. B. Sinclair, T. S. Luk, Sci. Rep.**6**, 34746 (2016).

[21] S. Vassant, J. –P. Hugonin, F. Marquier, J. –J. Greffet, Opt. Express **20**, 23971-23977 (2012).

[22] S. Vassant, A. Archambault, F. Marquier, F. Pardo, U. Gennser, A. Cavanna, J. Pelouard, J.-J. Greffet, Phys. Rev. Lett. **109**, 237401 (2012).

[23] S. Campione, I.l Brener, F. Marquier, Phys. Rev. B **91**, 121408 (2015).

[24] K. Kliewer, R. Fuchs, Phys. Rev. **153**, 498-512 (1967).

[25] A. McAlister, E. Stern, Phys. Rev. **132**, 1599-1602 (1963).

[26] D. W. Berreman, Phys. Rev. **130**, 2193-2198 (1963).

[27] G. V. Naik, V. M. Shalaev, A. Boltasseva, Adv. Mater.**25**, 3264-3294 (2013).
[28] T. Gric, O. Hess, J. Appl. Phys.**122**, 193105 (2017).
[29] O. Takayama, D. Artigas, L. Torner, Opt. Lett.**37**, 4311 (2012).
[30] 30.I. Iorsh, A. Orlov, P. Belov, Y. Kivshar, Appl. Phys. Lett.**99**(15), 151914 (2011).

Citation: *Tatjana Gric. "Review of Surface Plasmon Polaritons in Nanostructured Metamaterials", International Journal of Research Studies in Electrical and Electronics Engineering, 4(3), pp 18-25. DOI: http://dx.doi. org/10.20431/2454-9436.0403003*